Electrochemical deposition of ZnO thin films in aprotic ionic liquids: Effect of the cationic alkyl-chain-length

Rita Khalil, Mirella Azar, Ibrahim Bou Malham, Mireille Turmine, Vincent Vivier

Journal of Ionic Liquids 2 (2022) 100031

Contents lists available at ScienceDirect

Journal of Ionic Liquids

journal homepage: www.elsevier.com/locate/jil

Electrochemical deposition of ZnO thin films in aprotic ionic liquids: Effect of the cationic alkyl-chain-length

Rita Khalil[a,b,*], Mirella Azar[a], Ibrahim Bou Malham[a], Mireille Turmine[b,1], Vincent Vivier[b,1]

[a] Lebanese University, Faculty of Sciences IV, Laboratoire Énergétique à l'Échelle Nanométrique (EREN), Haouch El-Omara, Zahleh, Lebanon
[b] Sorbonne University, CNRS, Laboratoire Interfaces et Systèmes Électrochimiques (LISE), UMR 8235, 4 Place Jussieu, Paris 75005, France

ARTICLE INFO

Keywords:
Zinc oxide
Ionic liquids
Cationic alkyl chain
Electrodeposition

ABSTRACT

Zinc oxide (ZnO) is a semiconductor with various physicochemical properties allowing its use in a wide range of technological applications. The aim of this work is to study nanocrystalline ZnO thin-film deposited using zinc salt which is dissolved in pure ionic liquids (ILs). The latter play a dual role: solvent and supporting electrolyte. Most of ILs have a large electrochemical window and sufficient ionic conductivity. In this work, four hydrophobic ILs, based on 1-alkyl-3-methylimidazoliums bis(trifluoromethylsulfonyl)imide were synthetized and characterized to highlight the effect of the length of the cationic alkyl chain on the morphological, structural and optical properties of nanocrystalline ZnO deposits. Grain growth and its arrangement are affected by the length of the cation alkyl chain of ILs, that act as model agents during electroplating. The electrochemical properties of the produced thin layers were also studied.

Introduction

Over the past several years, the use of ionic liquids (ILs) in a large variety of fields has grown rapidly. Particularly, they have appeared as versatile media for synthesis and deposition of inorganic materials (Azaceta et al., 2011, 2013a; Yao et al., 2019) by different techniques such as solvothermal (Biswas and Rao, 2007), ionothermal (Tarascon et al., 2009) and electrochemical deposition (Azaceta et al., 2009; Maniam and Paul, 2020; Rivas-Esquivel et al., 2017; Maniam and Paul, 2021; Thomas et al., 2020).

Recently, ILs have been widely used for electrodeposition of semiconductors (Endres et al., 2008; Borisenko, 2015; Armand et al., 2009; Bakkar and Neubert, 2020; Kowalski et al., 2017). In fact, their broad electrochemical window (Khalil et al., 2020; Thiebaud et al., 2018), sufficient ionic conductivity (Thawarkar et al., 2020, 2019a), extremely low vapour pressures and good thermal stability (Huddleston et al., 2001) allowed their use as electrolytes for electrodeposition of zinc oxide at high temperatures (i.e., above 100 °C). In addition, the aprotic character of some ILs avoids the problems caused by the presence of hydronium ions (Klingshirn et al., 2007) that leads to the formation of hydrogen bubbles (Eshetu et al., 2016) during the electrolysis. It thus results in deposits with better mechanical properties (Peulon and Lincot, 1998; Wang, 2004; Izaki and Omi, 1996). ILs also have particular self-assembling properties and can be used as template agents. They are an important source of ions which interact with the inorganic solid surface (Azaceta et al., 2013b).

Zinc oxide is a promising material for numerous technological applications, because of its multi-functionality (Klingshirn et al., 2007) and its rich family of nanostructures (Wang, 2004). However, a better control of specific properties, especially the surface state, is still necessary to tune ZnO properties.

ZnO electrodeposition is presented as a relatively inexpensive and simple technique. In fact, the crystal structure and the thickness of the deposited thin film can be adjusted by modifying parameters such as the electrolyte composition, the potential of the electrode, the current density and the temperature (Torriero, 2015).

Peulon and Lincot (1998, 1996) have carried out in 1996, for the first time, the cathodic electrodeposition of ZnO in an aqueous electrolyte saturated with O_2 and containing zinc salt. In some conditions, oxygen can be removed as reported by Izaki and Omi (1996, 1997) who performed the ZnO electrodeposition from an aqueous solution of zinc nitrate. Some studies have also been performed in non-aqueous solutions such as polypropylene carbonate (O'Regan et al., 2001), dimethylsulfoxide (Gal et al., 2000) and ILs (Azaceta et al., 2011, 2009, 2013b; Tulodziecki et al., 2012).

In 2009, Azaceta et al. (2009) used an aprotic IL, 1-butyl-1-methylpyrrolidinium bis(trifluoromethylsulfonyl)imide ($PYR_{14}TFSI$), saturated with O_2 and containing $Zn(TFSI)_2$ as the zinc salt for electro-

* Corresponding author at: Laboratoire Énergétique à l'Échelle Nanométrique (EREN), Lebanese University, Faculty of Sciences IV, Haouch El-Omara, Zahleh, Lebanon.
E-mail address: ritamkhalil@hotmail.com (R. Khalil).
[1] Present address: Sorbonne University, CNRS, Laboratoire de Réactivité de Surface (LRS), UMR 7197, 4 Place Jussieu, 75005, Paris, France.

https://doi.org/10.1016/j.jil.2022.100031
Received 21 January 2022; Received in revised form 15 April 2022; Accepted 16 April 2022

plating ZnO at a constant potential of −1.6 V (vs. Fc/Fc^+) at 100 °C. ZnO film was the result of the reaction between Zn^{2+} and O_2^- released by O_2. The resulting films have shown a semiconducting behaviour and photoluminescent emissions at room temperature. The authors also have studied the effect of temperature and concentration of zinc salt on the morphology and crystal structure of the electrodeposited ZnO (Azaceta et al., 2011). Doan et al. (2012) have performed a zinc deposit using $PYR_{14}TFSI$ with $Zn(TFSI)_2$ as electrolyte, the zinc deposit was oxidized by air at high temperature. Tulodziecki et al. (2012) have also electrodeposited ZnO in two ILs of different nature, one hydrophobic, 1-ethyl-3-methylimidazolium bis(trifluoromethylsulfonyl)imide and the other hydrophilic, 1-butyl-3-methylimidazolium trifluoromethylsulfonate.

In the present work, ZnO films were prepared in 1-alkyl-3-methylimidazoliums bis(trifluoromethylsulfonyl)imide. The anion, bis(trifluoromethylsulfonyl)imide ($TFSI^-$), gives to the IL a low melting temperature, low viscosity (with respect to other ILs) and hydrophobic property. For the cations, an imidazolium family was chosen, providing a wide electrochemical window and a good conductivity to the ILs, in particular for the 1-alkyl-3-methylimidazolium. Few data are available on the electrodeposition of ZnO in imidazolium salts (Azaceta et al., 2011, 2013a, 2009; Tulodziecki et al., 2012; Doan et al., 2012). The morphology and structural properties of the obtained thin layers were also analysed, emphasizing the differences with respect to those obtained in aqueous and conventional organic electrolytes. Then the nature and quality of the nanostructured ZnO thin-layers will be discussed as a function of the physicochemical properties of the ILs used.

Experimental

Synthesis of the ILs $c_n$mimtfsi (n = 2; 4; 8 and 10) and zinc salt

The four ILs C_nMIMTFSI (n = 2; 4; 8 and 10) were used as electrochemical media. They were synthesized according to a standard procedure previously described in the literature (Yao et al., 2019; Khalil et al., 2020; Suarez et al., 1996). ILs, 1-alkyl-3-methylimidazoliums bis(trifluoromethylsulfonyl)imide, were prepared by anion exchange (Thawarkar et al., 2019b) from the corresponding bromide salts of imidazolium cations with different length of the n-alkyl chain, with lithium bis(trifluoromethylsulfonyl)imide (LiTFSI). Traces of water and other solvents were removed by freeze-drying for 24 h. The four ILs were stored in an argon-circulating glove-box. Structures of the resulting salts were confirmed by ^1H NMR spectroscopy and mass spectroscopy. The water content of each IL was quantified by Karl Fischer titration and was found to be less than 20 ppm. Zinc (II) bis(trifluoromethylsulfonyl)imide $Zn(TFSI)_2$ was synthesized by reaction of a solution of bis(trifluoromethylsulfonyl)imide acid (HTFSI) with an over-stoichiometric amount of zinc oxide powder in deionized water (Nie et al., 1997). The mixture was stirred over 48 h until no more oxide was consumed. The remaining solid was filtrated out. The water was evaporated and the resulting white powder was dried using freeze-drying for 48 h. $Zn(TFSI)_2$ was identified by mass spectrometry.

Electrodeposition of ZnO

ZnO films were deposited in a three-electrode electrochemical cell immersed at a hot silicon oil bath at 150 °C. The fluorine doped tin oxide coated glass substrate (FTO) was the working electrode. The counter electrode was a zinc bar to balance the consumption of Zn^{2+} ions at the cathode during the deposition procedure. The reference electrode consisted in an Ag wire immerged in a saturated solution of IL with $AgNO_3$. A second junction containing pure IL was added. Thus, the reference electrode was based on the couple $Ag/AgNO_3$.

The conductive substrate consisted in fluorine tin oxide sheet (FTO), which was cleaned according to the protocol described in the literature (Goux et al., 2005). It was immersed in an acetone container placed in an ultrasonic bath for 5 min. This operation was renewed by replacing acetone by pure ethanol. After extensive wash with water, FTO was immersed for 2 min in 45% nitric acid in the ultrasonic bath. It was rinsed with deionized water and then air dried.

The electrolyte was a 50 mmol L^{-1} of $Zn(TFSI)_2$ in IL, saturated with O_2. The solution was bubbled with oxygen before and during the electroplating.

The electrochemical measurements were carried out with a GAMRY RF600+ potentiostat. All the electrodepositions were carried out at a constant potential (−1.6 $V/Ag/AgNO_3$) during 2 h.

Physicochemical characterization

The morphology and crystalline structure of the films were analysed using a FEG-SEM ultra 55 Zeiss field emission scanning electron microscope and an Empyrean Panalytical X-ray diffractometer (XRD) using Cu Kα radiation (λ=1.5425 Å).

The optical transmittance was measured at room temperature using U-4001 Research-Grade, UV–Vis-NIR spectrophotometer from Hitachi, fitted with an integrating sphere (60 mm), from 300 to 500 nm.

Electrochemical performance

All the electrochemical measurements were performed with a three-electrode setup, in which the thin film of ZnO electrodeposited on the FTO substrate was the working electrode, a platinum grid was used as counter electrode and the Ag/AgCl in saturated KCl aqueous solution was the reference electrode. A 0.1 mol L^{-1} of KCl aqueous solution was used as electrolyte. The cyclic voltammetry was recorded with a potential range from 0 to 0.6 V/Ag/AgCl. The specific capacitance value C (F cm^{-2}) was calculated from the cyclic voltammograms using the following equation:

$$C = \frac{Q}{\Delta E S} \quad \text{(Eq. 1)}$$

where Q is the average charge during the charge and discharge processes, ΔE the potential window, and S the geometric surface area of the electrode.

The electrochemical impedance spectroscopy was performed in the 100 kHz to 0.1 Hz frequency range with a sinewave perturbation of 0.01 Vrms chosen so as to fulfil the stationarity and linearity of the system.

Results and discussion

First, cyclic voltammetry has been used to analyse the influence of each precursor (O_2 and $Zn(TFSI)_2$) and full electrolyte on the ZnO electrodeposition at 150 °C. In the second section, the physicochemical properties of the electrodeposited ZnO films were characterized in aqueous solution. The electrochemical performance of the films will be discussed in the last part.

Cyclic voltammetry

The electrochemical behaviour of each precursor (O_2 and $Zn(TFSI)_2$) in C_4MIMTFSI solution and the complete electrolyte were analysed by cyclic voltammetry, as showed in Fig. 1. Scans were performed at a rate of 50 mV s^{-1}. The electrolyte was a 50 mmol L^{-1} solution of $Zn(TFSI)_2$ in the IL, at 150 °C, in order to study the reaction and to determine the potential range at which the deposition can be carried out. All potential scans have been done with respect to the electrochemical window of the IL (Fig. S1).

For the IL saturated in oxygen by bubbling, during the cathodic sweep (blue curve in Fig. 1), a reduction wave appears towards −1.2 $V/Ag/AgNO_3$ (see insert of Fig. 1), followed by a significant decrease of the current density at about −1.7 $V/Ag/AgNO_3$. A small anodic wave was also observed around −1 $V/Ag/AgNO_3$. According to the previous studies by Katayama et al. (2004) and Evans et al. (2004), both

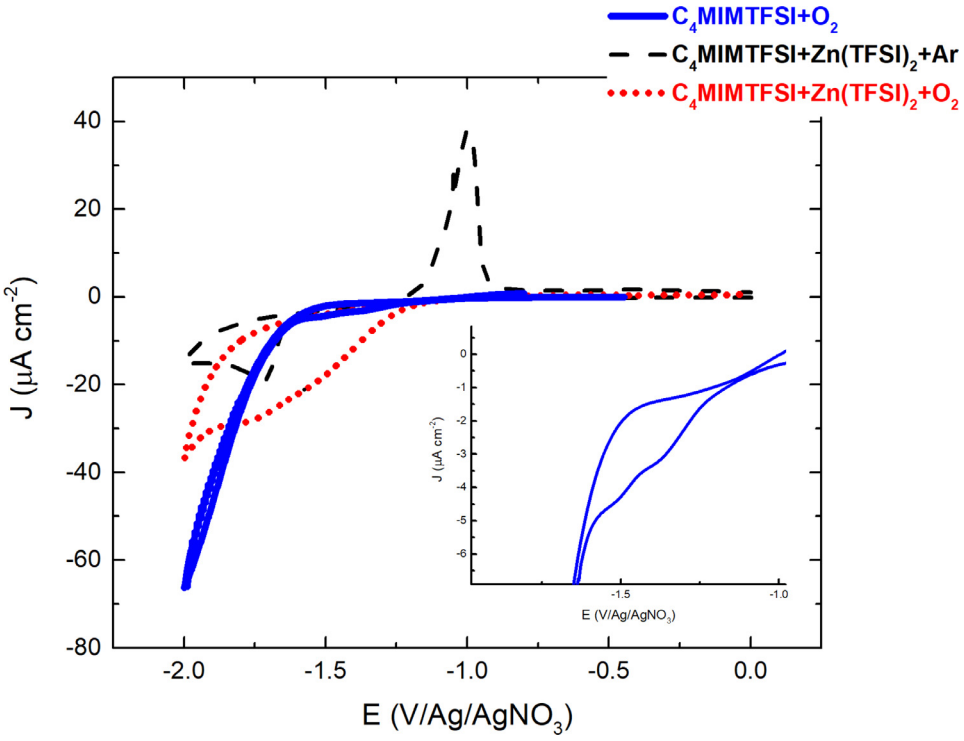

Fig. 1. Voltammograms of different solutions at 150 °C recorded at 50 mV s^{-1}: (full line) O_2 bubbled in C_4MIMTFSI, (dash line) $Zn(TFSI)_2$ dissolved in C_4MIMTFSI and (dot line) full electrolyte (C_4MIMTFSI+$Zn(TFSI)_2$ + O_2).

waves can be attributed to the O_2/O_2^- redox couple. The variation in cathodic current density at potentials below −1.7 V/ $Ag/AgNO_3$ may be ascribed to the reduction of O_2^- ions to O_2^{2-}.

For the solution containing the IL with 50 mmol L^{-1} $Zn(TFSI)_2$ under argon bubbling (black dashed curve in Fig. 1), the reduction of Zn^{2+} in metallic zinc, is observed and can be written as:

$$Zn^{2+} + 2e^- \rightarrow Zn \quad \text{(Eq. 2)}$$

During the cathodic sweep, the wave identifying the reduction of Zn^{2+} in Zn begins at −1.75 V/$Ag/AgNO_3$. During the backward sweep, an oxidation peak is observed, which corresponds to the dissolution of deposited Zn on the substrate.

Studying the full electrolyte (50 mmol L^{-1} $Zn(TFSI)_2$ in IL saturated in O_2) over the cathodic sweep, it is shown that the reduction wave starts around −1 V/$Ag/AgNO_3$ and is followed by a second wave around −1.7 V/$Ag/AgNO_3$ (red dotted curve in Fig. 1). The first one is ascribed to the reduction of O_2^-, which in presence of Zn^{2+}, leads to the following reaction:

$$Zn^{2+} + 2O_2^- \rightarrow ZnO_4 \quad \text{(Eq. 3)}$$

According to previous studies (Katayama et al., 2004), the second wave corresponds to the reduction of O_2^- to O_2^{2-}. The absence of Zn/Zn^{2+} signature during the anodic scan allows to rule out the reduction of Zn^{2+} during the cathodic sweep.

Thus, the stability of the redox couple O_2/O_2^- is disturbed in the presence of Zn^{2+} and the reaction that takes place with the generated O_2^- corresponds to a two-step mechanism which expresses as:

$$Zn^{2+} + 2O_2^- \rightarrow ZnO_4 \rightarrow ZnO + 3/2O_2 \quad \text{(Eq. 4)}$$

Similar CV curves were obtained for the whole family of ILs investigated in this work. They are presented in Figs. S2–S5. So, the electrodeposition of ZnO in the four ILs C_nMIMTFSI (n = 2; 4; 8 and 10) is possible and takes place following a different mechanism than what is usually observed in aqueous media because hydroxide ions are not involved and the superoxide anion is the reactive species.

Table 1
Thickness of electrodeposited films of ZnO in C_nMIMTFSI (n = 2, 4, 8 and 10) at 150 °C for 2 h.

IL	Thickness (nm)
C_2MIMTFSI	71.5 ± 1
C_4MIMTFSI	170.5 ± 1
C_8MIMTFSI	260.5 ± 1
C_{10}MIMTFSI	386.5 ± 1

Physicochemical properties of the films

Electrodepositions under potentiostatic conditions (E = −1.6 V/ $Ag/AgNO_3$) were performed at 150 °C for two hours, in each of the synthesized ILs with different length of the cationic alkyl chain. Transparent and uniform (at naked eye) films were obtained. The morphology of the deposited samples was studied by SEM (Fig. 2). They are compact and cover the entire surface that has been immersed in the electrolyte.

For a given set of parameters for the electroplating procedure, it is shown that the thickness of deposited ZnO increases with the length of the cationic alkyl chain of C_nMIMTFSI (Table 1).

In order to explain this result, we have to consider the peculiar properties of these ILs. Actually, the structures of some ILs can be similar to that of surfactants (Šarac et al., 2017). In fact, the 1-alky-3-methylimidazolium family has a marked amphiphilic character when the number of carbon in the cationic alkyl chain increases (Modaressi et al., 2007). This can lead to the formation of aggregates such as those formed by cationic surfactants. Indeed, ILs with long cationic chains have the ability to organize themselves and form micelles and lyotropic crystals in presence of water (Bowlas et al., 1996; Holbrey and Seddon, 1999; Allen et al., 2002; Firestone et al., 2002).

In fact, in alkylimidazolium-based ILs, a locally ordered non-polar phase is formed through the van der Waals force between the cationic alkyl chains (Wang and Voth, 2005). The adsorbed cations have been replaced by the discharged metal atoms. The replaced cations can adsorb

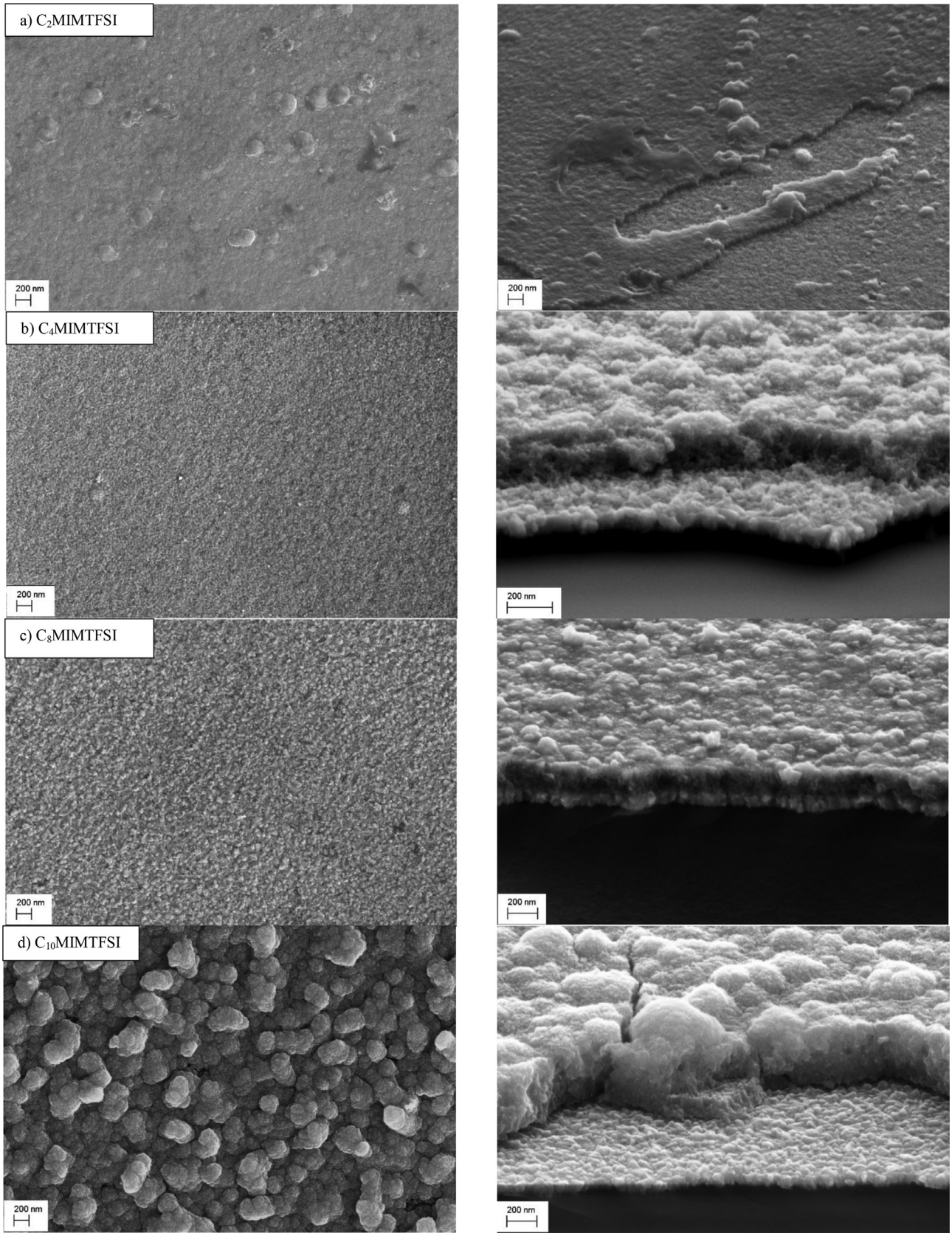

Fig. 2. SEM micrographs of the top view (left) and cross section (right) of ZnO electrodeposited at 150 °C for 2 h in (a) C_2MIMTFSI, (b) C_4MIMTFSI, (c) C_8MIMTFSI and (d) C_{10}MIMTFSI.

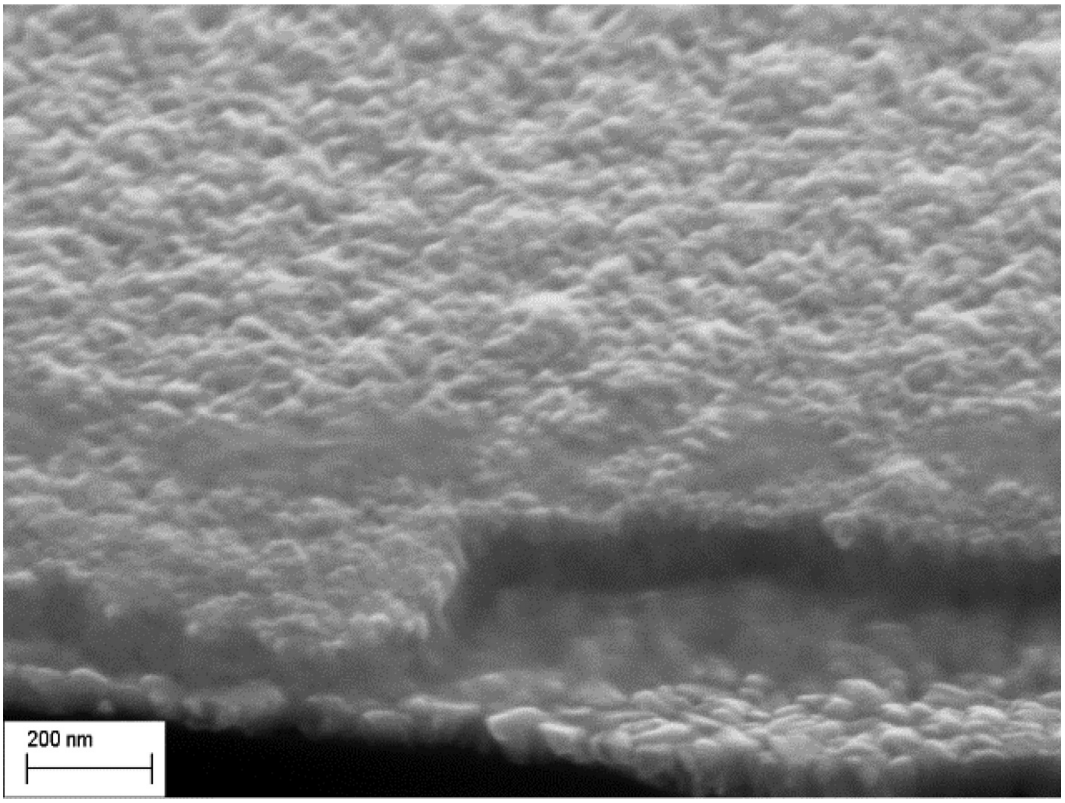

Fig. 3. SEM image of the cross section of ZnO film electrodeposited in the presence of the cationic surfactant in the C_4MIMTFSI at 60 °C for 2 h.

on top of deposited atoms, playing the role of surface surfactant: this is called "cation effect" (Su et al., 2010).

As a cathodic potential is applied to the substrate on which ZnO is deposited, the interface substrate-IL provides the required environment for the assembly of its components and the formation of adsorbates. Thereby, the polar head of the cation will be attracted by the substrate. The longer alkyl chains, the larger the non-polar areas. During polarization, Zn^{2+} ions will not be near the electrode, whatever the IL, because of the repulsion between cations of the IL and Zn^{2+} ions. It can be assumed that zinc salt is probably present in the non-polar region of the layers of IL near the substrate surface, allowing the reaction between Zn^{2+} in the IL and the O_2^- formed by the reduction of the dioxygen at the surface of the electrode. The results show that the longer alkyl chain, the better the reaction between Zn^{2+} and O_2^- (leading to thicker deposits).

In order to validate this hypothesis and show that the deposition of ZnO is enhanced by a layer of surfactants electrostatically adsorbed, ZnO deposits have been carried out in C_4MIMTFSI solution containing 50 mmol L^{-1} of $Zn(TFSI)_2$ and 0.1 mol L^{-1} of cationic or anionic surfactant saturated with O_2 at 60 °C, applying a potential of −1.6 V/Ag/$AgNO_3$ for two hours. At this temperature, there is no formation of ZnO in pure IL. This temperature has been chosen because surfactants degrade easily at higher temperatures. In the presence of anionic surfactant, sodium dodecylsulfate, no deposit could have been detected. On the other hand, when a cationic surfactant, the dodecyltrimethylammonium bromide, is used, a ZnO deposit with a thickness of about 109 nm is obtained as shown in Fig. 3. This illustrates the fact that in the IL, the electrodeposition of ZnO is enhanced by the existence of an amphiphilic cation layer adsorbed at the substrate surface.

In order to compare the robustness of ZnO thin films electrodeposited in ILs with respect to those realized in aqueous media, ZnO thin film electrodeposited in C_4MIMTFSI and a film of ZnO electrodeposited in aqueous media by Ghannam et al. (2018) were immersed in water for 12 h. As shown in Fig. 4, the ZnO electrodeposited in water disappeared completely after 12 h of immersion, while at the same time, ZnO thin film electrodeposited in the IL remains with some modifications. Thus, ZnO thin films electrodeposited in ILs display a certain robustness against water.

Fig. 5 displays the XRD patterns of the samples prepared in ILs. The characteristic diffraction peaks of wurtzite phase ZnO are observed indicating the ZnO electrodeposition. There is no preferential crystalline orientation. In fact, the (100), (002), (101) and (102) crystal planes located at 2θ values of 31.8°, 34.4°, 36.3° and 47.5°, respectively, are identified. The peaks that appear at 2θ values of 27° and 52° correspond to the FTO crystal structure.

Fig. 6 shows the optical transmittance spectra of ZnO samples electrodeposited in the four ILs with different length of cationic alkyl chain C_nMIMTFSI (n = 2, 4, 8 and 10). All samples showed high transparency (> 80%) in the visible range. The absorption coefficient A is related to the incident photon energy as

$$Ah\nu = \left(h\nu - E_g\right)^n \quad \text{(Eq. 5)}$$

where hν is the photon energy, E_g the bandgap and n is equal to $\frac{1}{2}$ for direct bandgap material such as ZnO. The bandgap was estimated from linear extrapolation of Eq. (5) as described by Tauc's model (Tauc et al., 1966; Thawarkar et al., 2021) .

Values in the range from 3.54 to 3.66 eV were obtained (Fig. 7), which are slightly higher than the usual value measured for ZnO at room temperature (3.37 eV), but confirming the semiconducting behaviour of samples. The band gap energy of ZnO thin films increases as the grain/crystallite size decreases. In fact, it has been found in previous works that band gap widening of nanomaterials are attributed to the quantum mechanical effects of the low dimensional crystallites (Kamarulzaman et al., 2015; Kumar and Sasikumar, 2014).

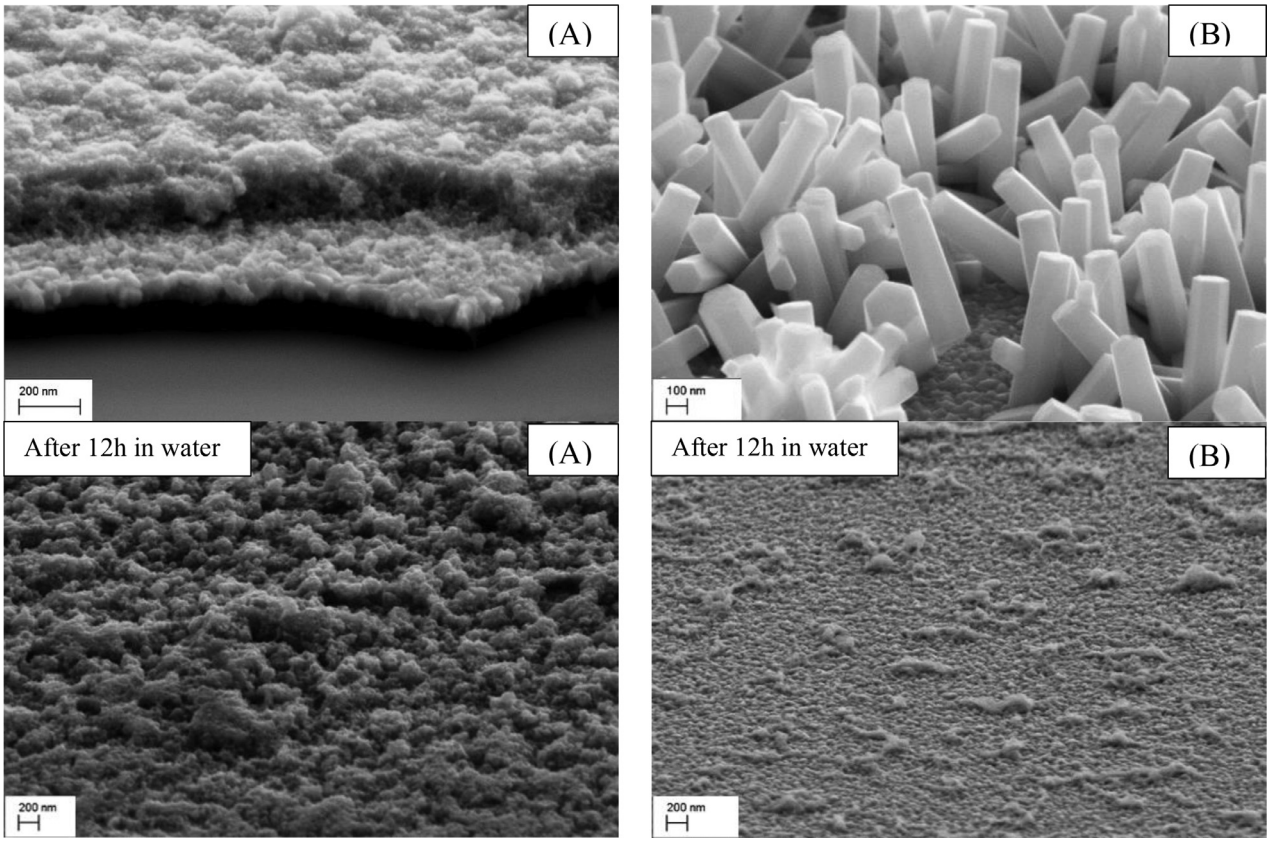

Fig. 4. SEM micrographs of ZnO electrodeposited in (A) C_4MIMTFSI and ZnO electrodeposited in (B) aqueous media, before (Top) and after (Bottom) 12 h in water.

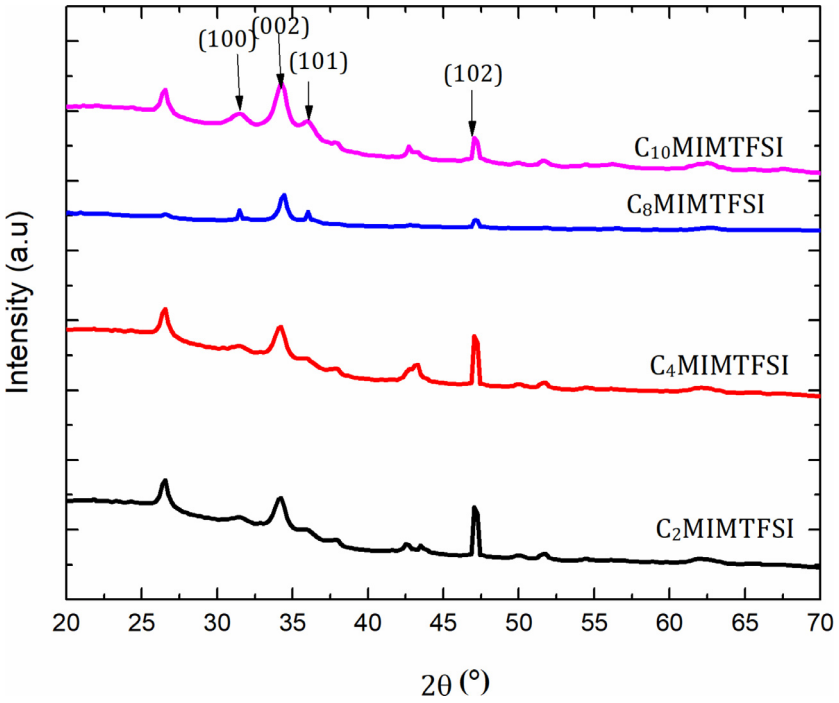

Fig. 5. XRD patterns of ZnO samples electrodeposited in C_nMIMTFSI (n = 2, 4, 8 and 10).

Electrochemical performance

In order to investigate the capacitive properties of these materials, each of the four electrodeposited ZnO thin films were used as the electrode materials.

Fig. 8 shows cyclic voltammograms performed in 0.1 M KCl aqueous solution for the different electrodeposited ZnO thin films. Scan rate is varied from 20 to 2000 mV s^{-1} at 25 °C. All of the electrodes have a rectangular symmetric shape for all scan rates. In fact, this CV shape is a signature of an ideal capacitive behaviour of electrode-electrolyte

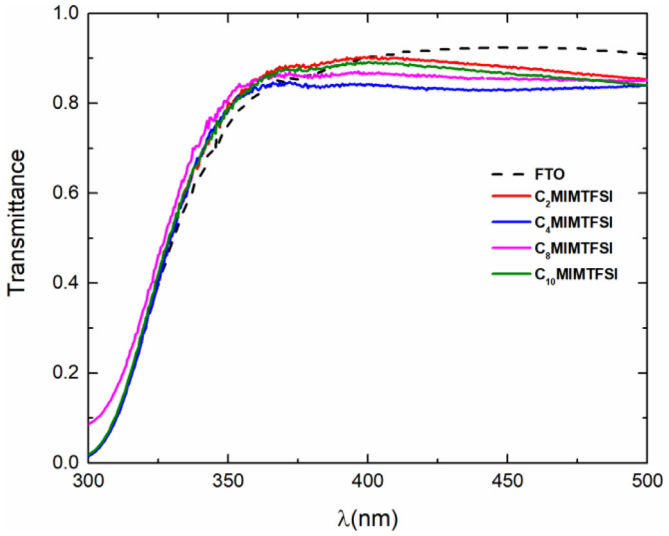

Fig. 6. Optical transmittance spectra of four samples electrodeposited in ionic liquids with different length of cationic alkyl chain C_nMIMTFSI (n = 2, 4, 8 and 10).

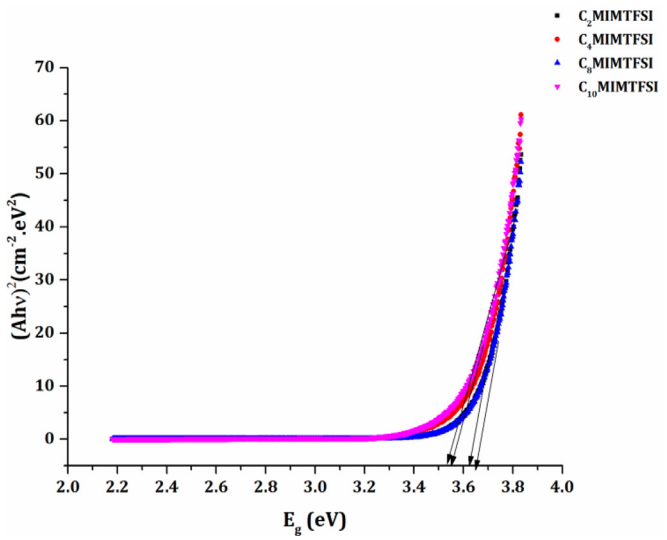

Fig. 7. Tauc's plot evaluated from UV–Vis absorption spectrum of the four samples electrodeposited in ionic liquids with different length of cationic alkyl chain C_nMIMTFSI (n = 2, 4, 8 and 10).

interface. No redox peak existed in the cyclic voltammograms during successive scans, resulting in an excellent electrochemical stability.

Fig. 9 shows the variation of the specific capacitance of the four electrodeposited thin films of ZnO as a function of the scan rate. All films exhibited a similar trend: a decreasing specific capacitance values as the scan rate increases. In fact, the increasing participation of the active surface area can justify the increase of the specific capac-

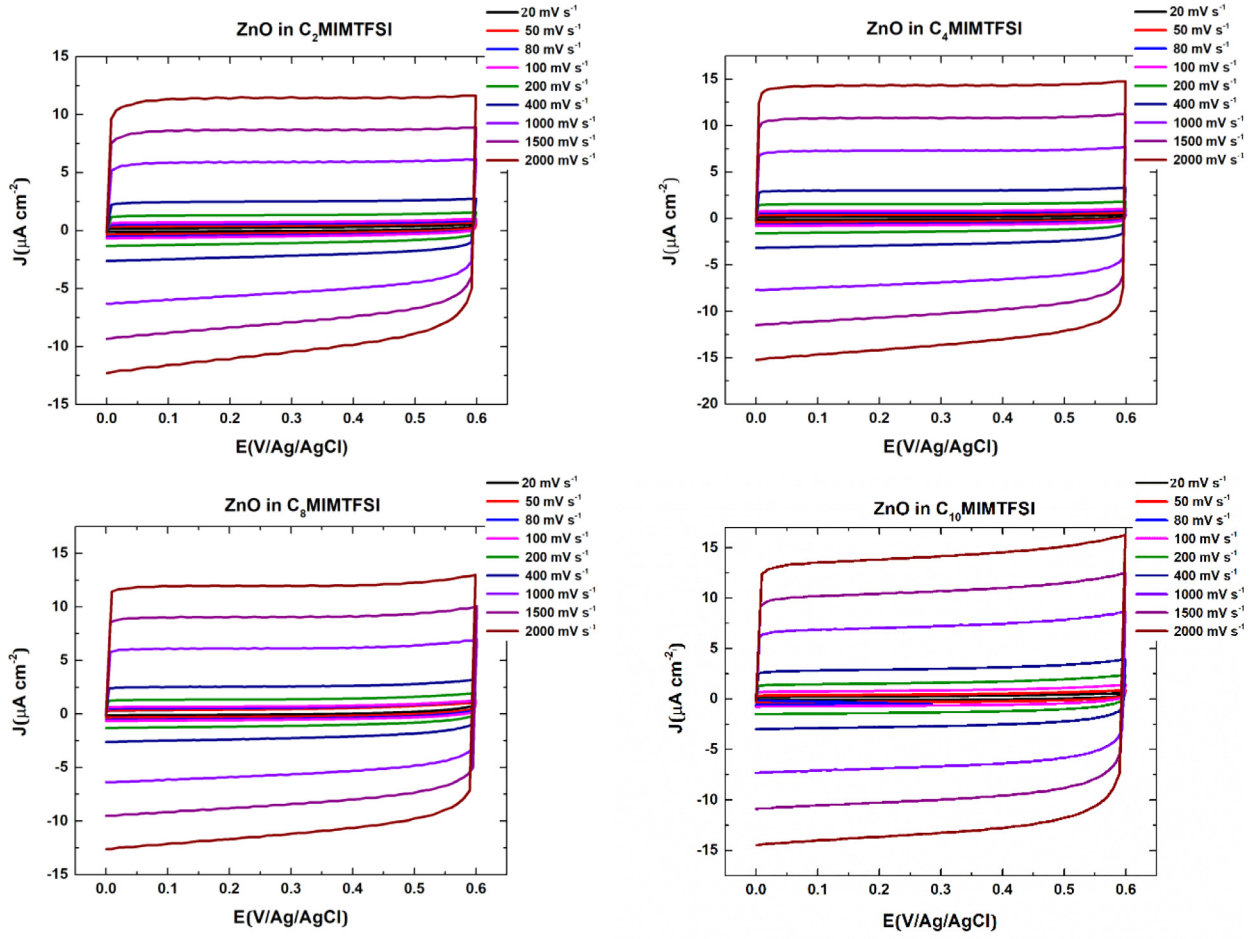

Fig. 8. Cyclic voltammograms of the electrodeposited thin films of ZnO in the four ILs at different scan rate in an aqueous solution of 0.1 mol L^{-1} KCl at 25 °C.

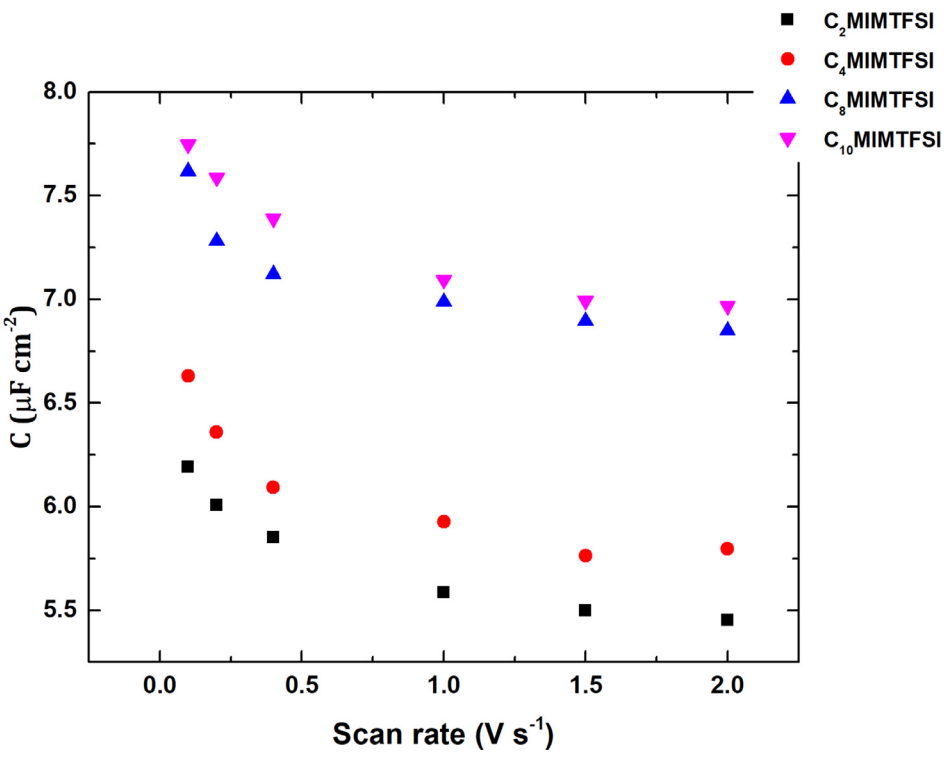

Fig. 9. Variation of the specific capacitance of ZnO films deposited in the four ILs with respect of the scan rate.

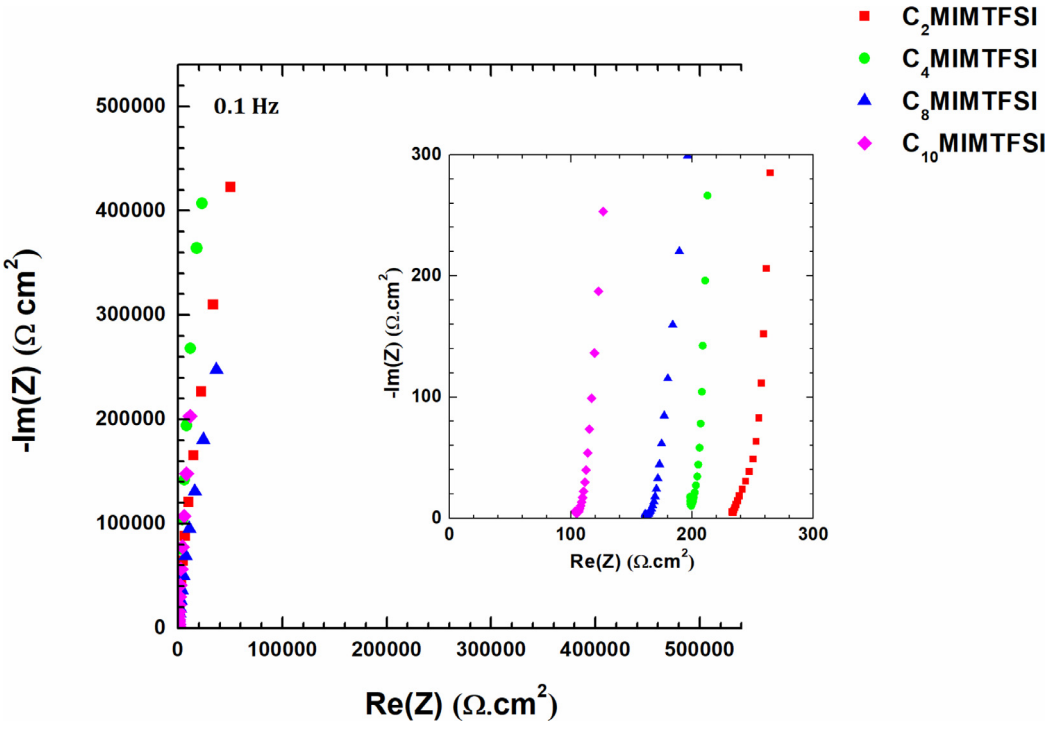

Fig. 10. Impedance spectroscopy measurements of ZnO samples electrodeposited in four ILs C_nMIMTFSI (n = 2, 4, 8, and 10) at 0.1 V/Ag/AgCl.

itance values at low scan rates. At a given scan rate, specific capacitance value of the deposit increases with the alkyl chain length. In other words, it increases when the thickness of deposit increases. As a prediction, thick deposits have larger active surface area than less thick layers.

An electrochemical capacitor electrode material should possess low electronic resistance (Zhou and Ma, 2015). In order to investigate this property, electrochemical impedance spectroscopy measurements have been performed for each of the four ZnO thin films. Fig. 10 shows the Nyquist plots of the four ZnO thin films, revealing a capacitive behaviour. At high frequencies, the intersection with the x-axis allows the determination of the sum of the electrolyte resistance and the resistance of the working electrode. At lower frequencies, the impedance plot should theoretically be a vertical line, which is parallel to the imaginary axis (Zhang et al., 2009). After determining the resistance of deposits at high frequencies (Table 2), these values remain relatively low

Table 2
Variation of the resistance and specific capacitance of the deposit as a function of the length of the alkyl chain.

ZnO in C_nMIMTFSI	R (Ω cm^2)	C (μF cm^{-2})
C_2MIMTFSI	233	3.8
C_4MIMTFSI	199	3.9
C_8MIMTFSI	162	6.4
C_{10}MIMTFSI	104	7.8

and decreases as the length of the cationic alkyl chain (or as the deposit thickness) increases.

At low frequencies, the specific capacitance values C (F cm^{-2}) (Table 2) were also calculated from the Nyquist diagram of the four electrodeposited ZnO thin films using the following equation

$$C = -\frac{1}{2\pi f \mathrm{Im}(Z)} \quad \text{(Eq. 6)}$$

where f is the lowest frequency (Hz) and $Im(Z)$ is the imaginary impedance at the lowest frequency (Ω cm^2). As expected, these values follow the trend of specific capacitance values calculated from cyclic voltammetry: the specific capacitance increases when the thickness of deposit increases. This is due to the increase of the electrode porosity/roughness that counter balance the effect of the increase of the deposit thickness, thus increasing the active surface area.

Conclusion

ZnO thin films with compact and robust morphology were electrosynthesized at 150 °C on FTO-coated glass substrates. Four ILs have been used as electrolyte in order to show the effect of the alkyl chain length on the quality of the electrodeposit. Thus, the longer the chain, the thicker the deposit, all experimental conditions being the same. The alkyl chain of the IL promotes the approach of the zinc cation to the substrate surface; the longer the chain, the greater the effect. Cyclic voltammetry has been performed to study the involved mechanism, identifying the formation of ZnO by the reaction between Zn^{2+} and O_2^-, delivered by O_2 reduction. The ZnO is formed in a different way than in the aqueous media and zinc hydroxides are not involved. The ILs moieties seem to affect the grain growth as well as their assembly in an important manner. Physicochemical properties (morphology, structure and optical properties) of the obtained films have been influenced by the alkyl chain: thicker films of ZnO have been obtained for longer cationic alkyl chain.

Declaration of Competing Interest

The authors declare that they have no known competing financial interests or personal relationships that could have appeared to influence the work reported in this paper.

Acknowledgments

The authors acknowledge the financial support of the Lebanese University, especially for the funding of Rita KHALIL. Stephanie DELBREL is thanked for FEG-SEM measurements and Cyrille BAZIN for XRD measurements.

Supplementary materials

Supplementary material associated with this article can be found, in the online version, at doi:10.1016/j.jil.2022.100031.

References

Armand, M., Endres, F., MacFarlane, D.R., Ohno, H., Scrosati, B., 2009. Ionic-liquid materials for the electrochemical challenges of the future. Nat. Mater. 8, 621.
Allen, D., Baston, G., Bradley, A.E., Gorman, T., Haile, A., Hamblett, I., Hatter, J.E., Healey, M.J., Hodgson, B., Lewin, R., 2002. An investigation of the radiochemical stability of ionic liquids. Green Chem. 4, 152–158.
Azaceta, E., Tena-Zaera, R., Marcilla, R., Fantini, S., Echeberria, J., Pomposo, J., Grande, H., Mecerreyes, D., 2009. Electrochemical deposition of ZnO in a room temperature ionic liquid: 1-Butyl-1-methylpyrrolidinium bis (trifluoromethane sulfonyl) imide. Electrochem. Commun. 11, 2184–2186.
Azaceta, E., Marcilla, R., Mecerreyes, D., Ungureanu, M., Dev, A., Voss, T., et al., 2011. Electrochemical reduction of O_2 in 1-butyl-1-methylpyrrolidinium bis (trifluoromethanesulfonyl) imide ionic liquid containing Zn^{2+} cations: deposition of non-polar oriented ZnO nanocrystalline films. Phys. Chem. Chem. Phys. 13, 13433–13440.
Azaceta, E., Tuyen, N.T., Pickup, D.F., Rogero, C., Ortega, J.E., Miguel, O., Grande, H.J., Tena-Zaera, R., 2013a. One-step wet chemical deposition of NiO from the electrochemical reduction of nitrates in ionic liquid based electrolytes. Electrochim. Acta 96, 261–267.
Azaceta, E., Idigoras, J., Echeberria, J., Zukal, A., Kavan, L., Miguel, O., Grande, H.-J., Anta, J.A., Tena-Zaera, R., 2013b. ZnO-ionic liquid hybrid films: electrochemical synthesis and application in dye-sensitized solar cells. J. Mater. Chem. A 1, 10173–10183.
Bakkar, A., Neubert, V., 2020. Electrodeposition of photovoltaic thin films from ionic liquids in ambient atmosphere: Gallium from a chloroaluminate ionic liquid. J. Electroanal. Chem. 856, 113656.
Biswas, K., Rao, C.e.N.e.R., 2007. Use of ionic liquids in the synthesis of nanocrystals and nanorods of semiconducting metal chalcogenides. Chem. A Eur. J. 13, 6123–6129.
Borisenko, N., 2015. Electrochemistry in Ionic Liquids. Springer, pp. 359–382.
Bowlas, C.J., Bruce, D.W., Seddon, K.R., 1996. Liquid-crystalline ionic liquids. Chem. Commun. 1625–1626.
Doan, N., Vainikka, T., Rautama, E.L., Kontturi, K., Johans, C., 2012. Electrodeposition of macroporous Zn and ZnO films from ionic liquids. Int. J. Electrochem. Sci. 7, 12034–12044.
Endres, F., MacFarlane, D., Abbott, A., 2008. Electrodeposition from Ionic Liquids. John Wiley & Sons.
Eshetu, G.G., Armand, M., Ohno, H., Scrosati, B., Passerini, S., 2016. Ionic liquids as tailored media for the synthesis and processing of energy conversion materials. Energy Environ. Sci. 9, 49–61.
Evans, R.G., Klymenko, O.V., Saddoughi, S.A., Hardacre, C., Compton, R.G., 2004. Electroreduction of oxygen in a series of room temperature ionic liquids composed of group 15-centered cations and anions. J. Phys. Chem. B 108, 7878–7886.
Firestone, M.A., Dzielawa, J.A., Zapol, P., Curtiss, L.A., Seifert, S., Dietz, M.L., 2002. Lyotropic liquid-crystalline gel formation in a room-temperature ionic liquid. Langmuir 18, 7258–7260.
Gal, D., Hodes, G., Lincot, D., Schock, H.W., 2000. Electrochemical deposition of zinc oxide films from non-aqueous solution: a new buffer/window process for thin film solar cells. Thin Solid Films 361, 79–83.
Ghannam, H., Bazin, C., Chahboun, A., Turmine, M., 2018. Control of the growth of electrodeposited zinc oxide on FTO glass. CrystEngComm 20, 6618–6628.
Goux, A., Pauporté, T., Chivot, J., Lincot, D., 2005. Temperature effects on ZnO electrodeposition. Electrochim. Acta 50, 2239–2248.
Holbrey, J., Seddon, K., 1999. Ionic liquids. Clean Prod. Process. 1, 223–236.
Huddleston, J.G., Visser, A.E., Reichert, W.M., Willauer, H.D., Broker, G.A., Rogers, R.D., 2001. Characterization and comparison of hydrophilic and hydrophobic room temperature ionic liquids incorporating the imidazolium cation. Green Chem. 3, 156–164.
Izaki, M., Omi, T., 1996. Transparent zinc oxide films prepared by electrochemical reaction. Appl. Phys. Lett. 68, 2439–2440.
Izaki, M., Omi, T., 1997. Transparent zinc oxide films chemically prepared from aqueous solution. J. Electrochem. Soc. 144, L3–L5.
Kamarulzaman, N., Kasim, M.F., Rusdi, R., 2015. Band gap narrowing and widening of ZnO nanostructures and doped materials. Nanoscale Res. Lett. 10, 1–12.
Katayama, Y., Onodera, H., Yamagata, M., Miura, T., 2004. Electrochemical reduction of oxygen in some hydrophobic room-temperature molten salt systems. J. Electrochem. Soc. 151, A59–A63.
Khalil, R., Chaabene, N., Azar, M., Malham, I.B., Turmine, M., 2020. Effect of the chain lengthening on transport properties of imidazolium-based ionic liquids. Fluid Phase Equilib. 503, 112316.
Klingshirn, C., Fallert, J., Zhou, H., Kalt, H., 2007. Comment on "Excitonic ultraviolett lasing in ZnO-based light emitting devices". Appl. Phys. Lett. 91, 131115.
Kowalski, D., Mallet, J., Thomas, S., Nemaga, A.W., Michel, J., Guery, C., Molinari, M., Morcrette, M., 2017. Electrochemical synthesis of 1D core-shell Si/TiO_2 nanotubes for lithium ion batteries. J. Power Sources 361, 243–248.
Kumar, M., Sasikumar, C., 2014. Electrodeposition of nanostructured ZnO thin film: a review. Am. J. Mater. Sci. Eng. 2, 18–23.
Maniam, K.K., Paul, S., 2020. Progress in electrodeposition of zinc and zinc nickel alloys using ionic liquids. Appl. Sci. 10, 5321.
Maniam, K.K., Paul, S., 2021. A Review on the Electrodeposition of aluminum and aluminum alloys in ionic liquids. Coatings 11, 80.
Modaressi, A., Sifaoui, H., Mielcarz, M., Domańska, U., Rogalski, M., 2007. Influence of the molecular structure on the aggregation of imidazolium ionic liquids in aqueous solutions. Colloids Surf. A 302, 181–185.
Nie, J., Kobayashi, H., Sonoda, T., 1997. Copper (II) bis ((trifluoromethyl) sulfonyl) amide. A novel Lewis acid catalyst in Diels-Alder reactions of cyclopentadiene with methyl vinyl ketone. Catal. Today 36, 81–84.

O'Regan, B., Sklover, V., Grätzel, M., 2001. Electrochemical deposition of smooth and homogeneously mesoporous ZnO films from propylene carbonate electrolytes. J. Electrochem. Soc. 148, C498–C505.
Peulon, S., Lincot, D., 1996. Cathodic electrodeposition from aqueous solution of dense or open-structured zinc oxide films. Adv. Mater. 8, 166–170.
Peulon, S., Lincot, D., 1998. Mechanistic study of cathodic electrodeposition of zinc oxide and zinc hydroxychloride films from oxygenated aqueous zinc chloride solutions. J. Electrochem. Soc. 145, 864–874.
Rivas-Esquivel, F., Brisard, G., Ortega-Borges, R., Trejo, G., Meas, Y., 2017. Zinc electrochemical deposition from ionic liquids and aqueous solutions onto indium tin oxide. Int. J. Electrochem. Sci. 12, 2026–2041.
Šarac, B., Medoš, Ž., Cognigni, A., Bica, K., Chen, L.J., Bešter-Rogač, M., 2017. Thermodynamic study for micellization of imidazolium based surface active ionic liquids in water: effect of alkyl chain length and anions. Colloids Surf. A 532, 609–617.
Su, Y.Z., Fu, Y.C., Wei, Y.M., Yan, J.W., Mao, B.W., 2010. The electrode/ionic liquid interface: electric double layer and metal electrodeposition. ChemPhysChem 11, 2764–2778.
Suarez, P.A., Dullius, J.E., Einloft, S., De Souza, R.F., Dupont, J., 1996. The use of new ionic liquids in two-phase catalytic hydrogenation reaction by rhodium complexes. Polyhedron 15, 1217–1219.
Tarascon, J.M., Recham, N., Armand, M., Chotard, J.N., Barpanda, P., Walker, W., Dupont, L., 2009. Hunting for better Li-based electrode materials via low temperature inorganic synthesis. Chem. Mater. 22, 724–739.
Tauc, J., Grigorovici, R., Vancu, A., 1966. Optical properties and electronic structure of amorphous germanium. Phys. Status Solidi 15, 627–637 (b).
Thawarkar, S., Khupse, N.D., Shinde, D.R., Kumar, A., 2019a. Understanding the behavior of mixtures of protic-aprotic and protic-protic ionic liquids: Conductivity, viscosity, diffusion coefficient and ionicity. J. Mol. Liq. 276, 986–994.
Thawarkar, S., Nirmale, T.C., More, S., Ambekar, J.D., Kale, B.B., Khupse, N.D., 2019b. Langmuir 35, 9213–9218.
Thawarkar, S., Khupse, N.D., Kumar, A., 2020. Binary mixtures of aprotic and protic ionic liquids demonstrate synergistic polarity effect: an unusual observation. J. Solut. Chem. 49, 210–221.
Thawarkar, S., Rondiya, S.R., Dzade, N.Y., Khupse, N., Jadkar, S., 2021. Experimental and Theoretical Investigation of the Structural and Opto-electronic Properties of Fe-Doped Lead-Free Cs2AgBiCl6 Double Perovskite. Chem. Eur. J. 27, 7408–7417.
Thiebaud, L., Legeai, S., Ghanbaja, J., Stein, N., 2018. Synthesis of Te-Bi core-shell nanowires by two-step electrodeposition in ionic liquids. Electrochem. Commun. 86, 30–33.
Thomas, S., Mallet, J., Bahuleyan, B.K., Molinari, M., 2020. Growth of homogeneous luminescent silicon–terbium nanowires by one-step electrodeposition in ionic liquids. Nanomaterials 10, 2390.
Torriero, A.A., 2015. Electrochemistry in Ionic Liquids. Applications 2 *Volume*.
Tulodziecki, M., Tarascon, J.M., Taberna, P., Guéry, C., 2012. Electrodeposition growth of oriented ZnO deposits in ionic liquid media. J. Electrochem. Soc. 159, D691–D698.
Wang, Y., Voth, G.A., 2005. Unique spatial heterogeneity in ionic liquids. J. Am. Chem. Soc. 127, 12192–12193.
Wang, Z.L., 2004. Zinc oxide nanostructures: growth, properties and applications. J. Phys. Condens. Matter 16, R829.
Yao, K., Zhai, M., Ni, Y., 2019. α-Ni $(OH)_2 \cdot 0.75\ H_2O$ nanofilms on Ni foam from simple $NiCl_2$ solution: Fast electrodeposition, formation mechanism and application as an efficient bifunctional electrocatalyst for overall water splitting in alkaline solution. Electrochim. Acta 301, 87–96.
Zhou, X., Ma, L., 2015. MnO_2/ZnO porous film: Electrochemical synthesis and enhanced supercapacitor performances. Thin. Solid. Films 597, 44–49.
Zhang, Y., Li, H., Pan, L., Lu, T., Sun, Z., 2009. Capacitive behavior of graphene–ZnO composite film for supercapacitors. J. Electroanal. Chem. 634, 68–71.